Journal of Materials Chemistry A

Accepted Manuscript

ROYAL SOCIETY OF CHEMISTRY

www.rsc.org/materialsA

Journal Name

ARTICLE

Sulfur synchronously electrodeposited onto exfoliated graphene sheets as cathode material for advanced lithium-sulfur batteries

Received 00th January 20xx,
Accepted 00th January 20xx

DOI: 10.1039/x0xx00000x

www.rsc.org/

Liyuan Zhang,[a] Hui Huang,[a,b,*] Hailin Yin,[a] Yang Xia,[a,b] Jianmin Luo,[a] Chu Liang,[a,b] Yongping Gan,[a] Xinyong Tao,[c] Wenkui Zhang[a,*]

Lithium-sulfur batteries show fascinating potential applications for the rapid-growing electric vehicles and grid-level energy storage due to low cost and high energy density. Up to date, various carbon hosts have been utilized to confine sulfur for improving Li-S battery performance. However, the adopted sulfur storage techniques are post-carbon-synthesis involving complex processes. It remains a great challenge for the ideal configuration of carbon-sulfur composite with uniform dispersion and high sulfur loading. Herein, we report a novel synthesis of graphene-sulfur composite by electrolytic exfoliation of graphite coupled with *in situ* sulfur electrodeposition. The sample delivers an initial discharge capacity of 1080 mAh g^{-1} at 0.1 A g^{-1} and retains above 900 mAh g^{-1} over 60 cycles. This strategy *via.* electrochemical exfoliation/deposition synchronous reactions can provide strong sulfur chemical interaction with the graphene host, achieving advanced cathode materials for Li-S batteries.

Introduction

Lithium-sulfur (Li-S) batteries have attracted increasing interests in recent years due to sulfur's high theoretical capacity (1675 mAh g^{-1}), abundance, low cost, and environmental benignity.[1–3] Despite these considerable advantages, sulfur cannot be solely used as the cathode material because of its low electrical conductivity (5×10^{-30} S cm^{-1} at 25 °C),[4] high solubility of polysulfide intermediates (Li_2S_n, $4\leq n\leq 8$) in the electrolyte and large volume expansion during discharge.[5] These issues cause poor cycle life, low specific capacity and low Coulombic efficiency of the Li-S batteries.

In order to solve these disadvantages, sulfur must be confined into conductive hosts with sulfur-locked function.[6] So far, there are mainly two categories of hosts reported to accommodate sulfur including carbon[7, 8] and conducting polymers.[9, 10] The most commonly adopted strategy is to incorporate sulfur into carbon hosts with porous structures or high specific surface area such as porous carbon,[11] hollow carbon spheres,[12] carbon nanotubes/fibers,[13–15] graphene (oxide)[16–20] and so on. The carbon hosts are believed to effectively contain sulfur and suppress the diffusion of polysulfides. Meanwhile, carbon framework greatly facilitates electron transport and promotes the redox processes in the electrode. Therefore, it can be assumed that the sulfur content, the homogeneous distribution and the binding of sulfur particles with carbon hosts, which are strongly dependent on the preparation methodology, would have significant influences on the electrochemical performance of carbon-sulfur composites. Currently, there has been a growing endeavors in developing synthesis methods with enhanced performance of carbon-sulfur composites. Many approaches have been achieved, for example, sulfur melting adsorption,[5] vapor phase infusion,[4, 21] solvent evaporation,[15, 20] sulfur precipitation[22] and deposition in the aqueous solutions.[17, 23] However, most traditional methods are post-carbon-synthesis and usually involve complex manufacturing processes. Moreover, this confining sulfur through architectural effect is limited by the structure and surface chemistry properties of carbon hosts, and generally cannot ensure uniform distribution of sulfur in the composites. Residual sulfur particles would remain within the carbon framework without being well encapsulated, which would dissolute in the electrolyte and suffer the shuttle problem. In particular, an advanced one-step method for the fabrication of sulfur-carbon composites is very attractive and promising.

The ideal configuration for carbon-sulfur composites is to have uniform dispersion and high sulfur content, complete sulfur enclosure in a confined, but accessible space, and strong sulfur-host affinity to achieve high capacity and excellent capacity retention. It is regret that the current methods do not meet this goal for the reason that the carbon materials are pre-existing or pre-prepared. As an effective strategy for the synthesis of nanostructured materials, electrodeposition method offers many advantages such as simplicity,

[a] College of Materials Science and Engineering, Zhejiang University of Technology, Hangzhou 310014, China

[b] State Key Lab of Silicon Materials & Department of Materials Science and Engineering, Hangzhou 310027, China Zhejiang University

[c] Department of Materials Science and Engineering, Stanford University, Stanford, California 94305, United States

*Corresponding authors. E-mail address: msechem@zjut.edu.cn

† Electronic Supplementary Information (ESI) available. See DOI: 10.1039/x0xx00000x

low cost and controllable deposition. Especially for carbon-sulfur composites, electrodeposition shows exclusive advantages over traditional methods. Firstly, that the sulfur electrodeposition reaction *via* electron/ion transfer at electrode/electrolyte interfaces can provide strong sulfur chemical bonding with carbon hosts. Secondly, this method can allow the incorporation of sulfur into the carbon structure and possibly even graphitic layers due to the penetration of the electrolyte into the material interior. Thirdly, sulfur is both electronically and ionically insulating. Once a thin sulfur layer covers the surface of carbon hosts, further electrodeposition reaction will be largely impeded, which avoids excessive deposition of sulfur on carbon hosts. Although the electrochemical preparation of sulfur nanoparticles have been achieved in the electrolytes such as sodium thiosulfate ($Na_2S_2O_3$),[24] and Na_2S,[25, 26] the elucidation of the redox processes of sulfur and sulfides is a very difficult task owing to the formation of polysulfide ions in the solution and at the electrode surface. To date, employing electrodeposition technique for preparing carbon-sulfur composites has not been reported yet.

As compared to other carbon materials, graphene makes it a potential matrix for Li-S batteries due to high surface area, good chemical stability, excellent mechanical strength and flexibility.[16-20] Shi *et al*.[27] synthesized a binder-free reduced graphene oxide-sulfur composite aerogel with a self-assembled compact reduced graphene oxide skin by hydrothermal method, showing an initial discharge capacity of 796 mAh g^{-1} and capacity retention of 81% after 250 cycles. Yang *et al*.[28] reported electrochemical assembly strategy to achieve ordered sulfur-graphene nanowalls. Inspired by the effective electrolytic exfoliation of graphite into graphene aggregates recently reported,[29–32] herein, we report a facile and novel strategy to synthesis graphene-sulfur composites (GSC) basing on a rational design of electrolytic exfoliation of graphite into graphene combined with *in situ* electrodeposition of sulfur as a one-pot reaction. The as-formed GSC electrode delivers an initial discharge capacity of 1080 mAh g^{-1} and retains more than 900 mAh g^{-1} over 60 cycles at 0.1 A g^{-1}, showing promising characteristics as a high-performance cathode material for Li-S batteries.

Experimental

Sample preparation

Figure 1 shows the schematic of the synthesis process. A high purity graphite rod anode (99.99%) was employed as the source of graphene for electrochemical exfoliation experiments. A Pt flake was chosen as the counter electrode. The electrolyte was obtained by mixing 4.8 g of sulfuric acid (98%), 0.3 g of KOH, 0.5 M sulfourea and 100 mL of deionized water. A constant voltage of 5 V was applied to two electrodes. During the electrolytic process, SO_4^{2-} and OH^- ions were intercalated into the grain boundary of graphite, where the graphite was expanded by gaseous species such as oxygen released from the oxidation of intercalants.[29] At the same time, sulfourea molecule could be infiltrated sufficiently into the expandable graphite layers, and *in situ* conversed into sulfur particles. The electrochemical exfoliation of graphite electrode and the electrodeposition of sulfur occur simultaneously, resulting in GSC being *in situ* formed. For comparison, pure sulfur was also prepared by a similar electrodeposition method in the same electrolyte solution. Instead of graphite rod, a Pt flake were used as the anode for sulfur preparation.

Materials characterization

The X-ray diffraction (XRD) of the sample was conducted on an X'Pert Pro diffractometer using CuKα radiation (λ=0.15418 nm). The morphology of the sample was characterized by scanning electron microscopy (SEM, Hitachi, S4700) and transmission electron microscopy (TEM, FEI, Tecnai G2 F30). Thermogravimetric analysis (TGA) was performed on a thermogravimetric analyzer (TGA, Q500, TA Instrument Corporation) in a flow of nitrogen with a heating rate of 10 ^oC min^{-1} from room temperature to 600 ^oC. Nitrogen adsorption-desorption isotherms were determined by Brunanuer-Emmett-Teller (BET) test using an ASAP 2020 (Micromeritics Instruments) surface area and pore analyzers.

Electrochemical measurements

Electrochemical performances of GSC and pure sulfur were evaluated by using a CR2025-type coin cell. The electrode was comprised of 70 wt.% active material, 20 wt.% Super-P and 10 wt.% polyvinylidene fluoride (PVDF) binder with N-methyl-2-pyrrolidinone (NMP) as dispersant. The slurry was coated onto an aluminum foil and dried at 60 ^oC for 24 h to remove the residual solvent. The loading mass of GSC or pure sulfur in the electrode sheet was about 0.8 mg in a square centimeter of aluminum foil (~0.8 mg cm^{-2}). The half-cell was assembled in an argon-filled glove box, using a lithium foil as the counter electrode and a Celgard membrane as the separator. The electrolyte solution was 1 M $LiN(CF_3SO_2)_2$ (LiTFSI; 99.95% trace metals basis) dissolved in a mixture of 1,3-dioxolane (DOL) and dimethoxymethane (DME) (1:1 by volume). Cyclic voltammetry (CV) measurements were performed on a CHI650B electrochemical workstation (Shanghai Chenhua, China) between 1.5 and 3.0 V at a scan rate of 0.1 mV s^{-1}. Galvanostatic charge/discharge experiments were conducted on

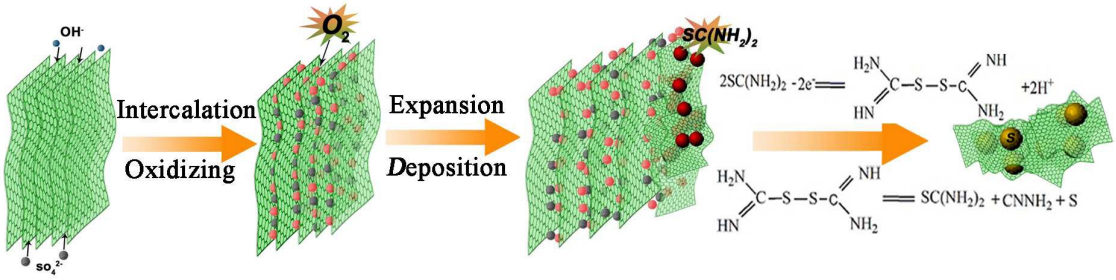

Figure 1. Schematic diagrams showing electrochemical exfoliation of graphite coupled with *in situ* sulfur intercalation to form GSC.

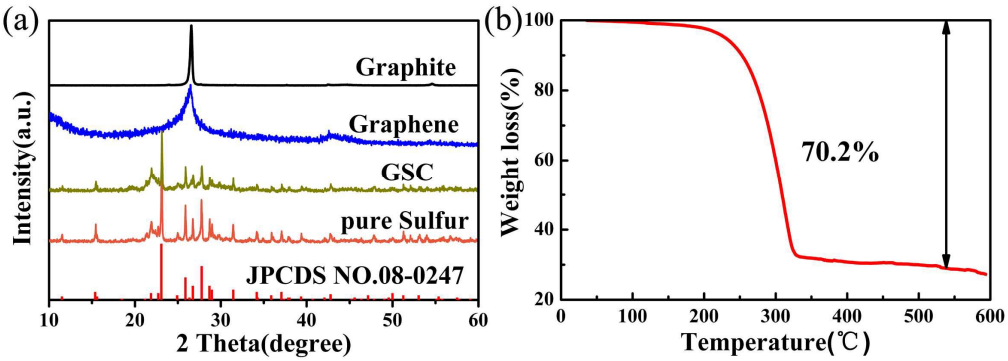

Figure 2. (a) XRD patterns of samples. (b) TGA curve of GSC.

Neware battery test system at different rates. All of the electrochemical performance measurements were obtained at ambient temperature.

Results and discussion

Figure S1 (Supporting Information) shows the cyclic voltammetry curves of the graphite electrode in the electrolytes with or without the addition of sulfourea. During the anodic scanning in the electrolyte with sulfourea, two well-defined peaks corresponding to the electrooxidation of sulfourea are observed, confirming that the electrodeposition of sulfur occurs. The detailed mechanism was not understood yet and could be due to the complex electrode reaction processes, which is needed to elucidate in the future work.

After electrolysis, the GSC in the form of fine gray powders was characterized by X-ray diffraction (XRD) and compared to the pristine graphite electrode and the graphene prepared by electrolytic exfoliation of graphite in the electrolyte without adding sulfourea (Figure 2a). The XRD pattern of graphite shows a sharp peak at 2θ=26.6° corresponding to the diffraction of (002) plane with interlayer distance of ~0.34 nm. By comparison, the (002) peak for the graphene becomes broader and weaker, indicating that the as-exfoliated graphene has graphite-like structure but with larger interplanar distance than the pristine graphite. The XRD pattern of pure sulfur exhibits some sharp and strong peaks throughout the diffraction range, indicating a well-defined crystal structure. To compare with the peaks of pure sulfur, the peaks of crystalline sulfur of GSC are detected throughout the entire diffraction range, indicating that elemental sulfur is formed in the GSC (JCPDS no. 08-0247). The content of sulfur in the GSC can be determined by thermogravimetric analysis (TGA). As calculated from the TGA curve in Figure 2b, the content of sulfur reaches as high as 70.2 wt%. The amount is significantly higher than that of the reported graphene-sulfur or carbon-sulfur composites synthesized by other methods, as summarized by Wang *et al*,[33] indicating that the high sulfur content can be achieved by this facile *in situ* electrodeposition method.

The Raman spectra of the GSC and graphene are presented in Figure S2. The Raman spectra of GSC and graphene display two prominent peaks at 1350 and 1585 cm^{-1}, which correspond to the A_{1g} vibration mode of the disordered carbon (D band) and the E_{2g} vibration mode of the ordered graphitic carbon (G band), respectively. The intensity ratio of D to G band (I_D/I_G) indicates the graphitization degree of carbon. The graphene spectrum denotes an evident characteristic of partially graphitic content (I_D/I_G is close to 0.84). The I_D/I_G ratio of the GSC is 1.05, which is larger than that of graphene. The increase of the I_D/I_G ratio is ascribed to the unavoidable defects or disorders at the connection spots between the graphene and sulfur particles. Figure S3 shows the Nitrogen adsorption-desorption isotherm of GSC. It can be calculated that the BET specific surface area of GSC is about 10.19 $m^2 g^{-1}$.

X-ray photoelectron spectroscopy (XPS) was used to characterize the chemical state of sulfur in the GSC. Figure 3a shows the S 2p XPS spectra of the GSC. Various sulfur bonds can be observed. The peaks at 163.8 and 165.0 eV are assigned to C-S

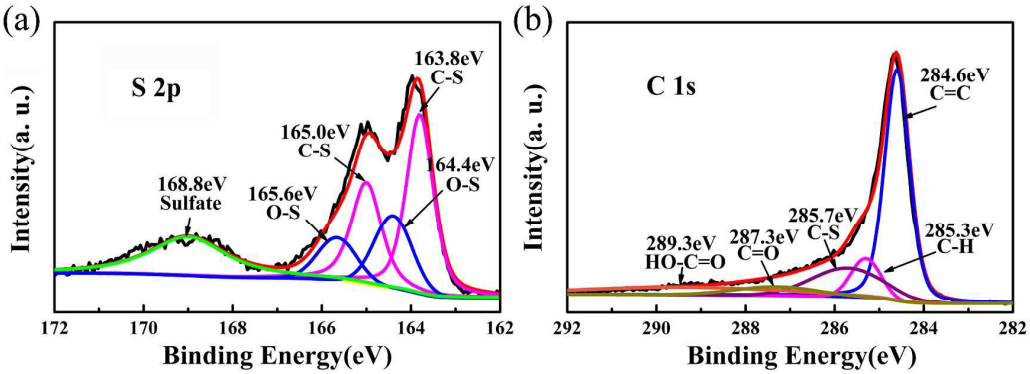

Figure 3. XPS S 2p (a) and C 1s (b) spectra of GSC.

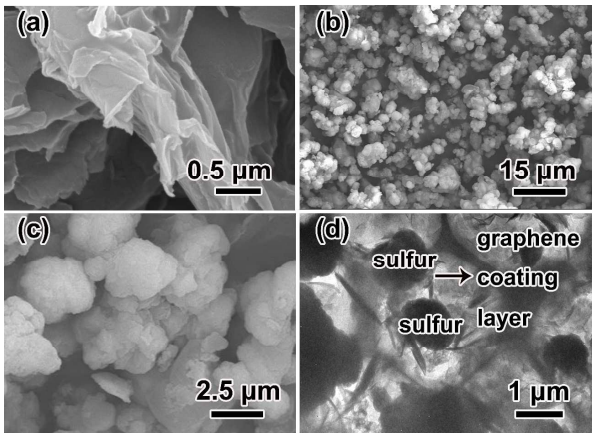

Figure 4. (a) SEM image of graphene sheets. (b) low- and (c) high magnification SEM images of GSC. (d) TEM image of GSC.

species. The peaks at 164.4 and 165.6 eV correspond to O-S species.[34–36] In addition, a weak broad peak centered at 168.8 eV is observed, which is ascribed to the sulfate species from the remaining precursor during electrochemical exfoliation-deposition reactions or from the oxidized sulfur in air.[34] The C1s spectra in Figure 3b displays an obvious characteristic peak of the sp2 carbon (C=C) at 284.6 eV. The small peaks at 285.7 and 285.3 eV can be assigned to C-S and C-H bonds, respectively.[37–39] The weak peaks at 287.3 and 289.3 eV can be ascribed to hydroxyl (C=O), carboxyl (HO-C=O) groups, respectively, which is likely due to the oxidation and destruction of graphite rod anode.[37, 39]

The microstructure of the samples was characterized by scanning electron microscopy (SEM) and transmission electron microscopy (TEM). Figure 4a shows a typical SEM image of the electrolytic exfoliated graphene, which are rippled and entangled with an interesting stacking structure. The internal space between the stacked graphene layers offers enough room for sulfur storage. Figure 4b shows the SEM image of the GSC. The sulfur particles show a uniform size distribution with the size of 1–3 μm. Figure 4c-d clearly present that the graphene sheets are coating around the sulfur particles. This facile electrochemical exfoliation-deposition strategy enables us to obtain uniform and fine graphene-wrapped sulfur particles.

The STEM image of GSC is presented in Figure 5a. It indicates that sulfur particles are well enfolded by graphene sheets. To verify the structure and composition of GSC, we carried out energy dispersive spectroscopic (EDS) mapping/imaging of our material. Figure 5c-d exhibit chemical mapping of sulfur and carbon of the region shown in Figure 5b. The sulfur and carbon mappings match well with the STEM image in Figure 5b, indicating that sulfur and carbon are homogeneously distributed throughout the composites.

The initial lithiation/delithiation behavior of the GSC and pure sulfur electrodes were characterized by the CV curves. Figure 6a and b show the CV curves of the GSC and pure sulfur electrodes. As shown in Figure 6a, two well-defined peaks of GSC are clearly observed in the cathodic scan, demonstrating that the

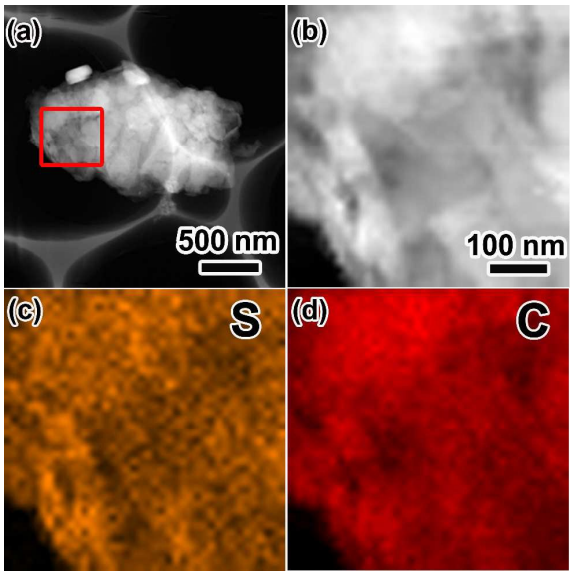

Figure 5. (a-b) STEM images of GSC. (c-d) EDS sulfur and carbon mapping of the region shown in (b).

electrochemical reduction of sulfur occurs in two stages. The first peak at ~2.26 V is assigned to a fast kinetic process, involving the open ring reduction of cyclic S_8 to the long-chain lithium polysulfides (Li_2Sn) ($4 \leq n \leq 8$),[1] the second peak at ~2.02 V corresponds to the conversion of lithium polysulfides to low-order Li_2S_2 and eventually to Li_2S. In the anodic scan, only one oxidation peak at ~2.42 V can be observed that is attributed to the conversion of Li_2S and polysulfides to elemental S. Compared to the CV curves of pure sulfur (Figure 6b), the cathodic and anodic peaks of GSC are well overlapped after initial several CV cycles, suggesting that the GSC can effectively accommodate the volume change during reversible electrochemical reaction and protect intercalated sulfur from dissolution.

Figure 6c shows the cycling performance of the GSC electrode at 0.1 A g^{-1}. The capacity is calculated basing on the mass of sulfur in the electrode. The GSC exhibits a relatively stable capacity during charge-discharge cycling. The discharge capacity of the first and second cycle is 1080 mAh g^{-1} and 943 mAh g^{-1}, respectively. After 60 cycles, the GSC still maintains high capacity of ~900 mAh g^{-1} with the capacity retention of 95.4% (which is calculated on the basis of the discharge capacity data of the 60th cycle and the second cycle) and Coulombic efficiency of 98%. The capacity fade is most likely due to the formation of insulating domains of Li_2S that are not fully oxidized upon charge of the cell, and not due to the active mass loss from polysulfides dissolution.[40, 41] It can be deduced that the sulfur confined into graphene layers by electrochemical exfoliation-deposition synchronous method is responsible for stable reversible capacities due to both physical confinement and chemical interaction. Unlike traditional methods relying on the diffusion of sulfur into the graphene framework, our *in situ* electrodeposition can allow sulfur further into graphitic layers because the sulfourea molecule can sufficiently penetrate

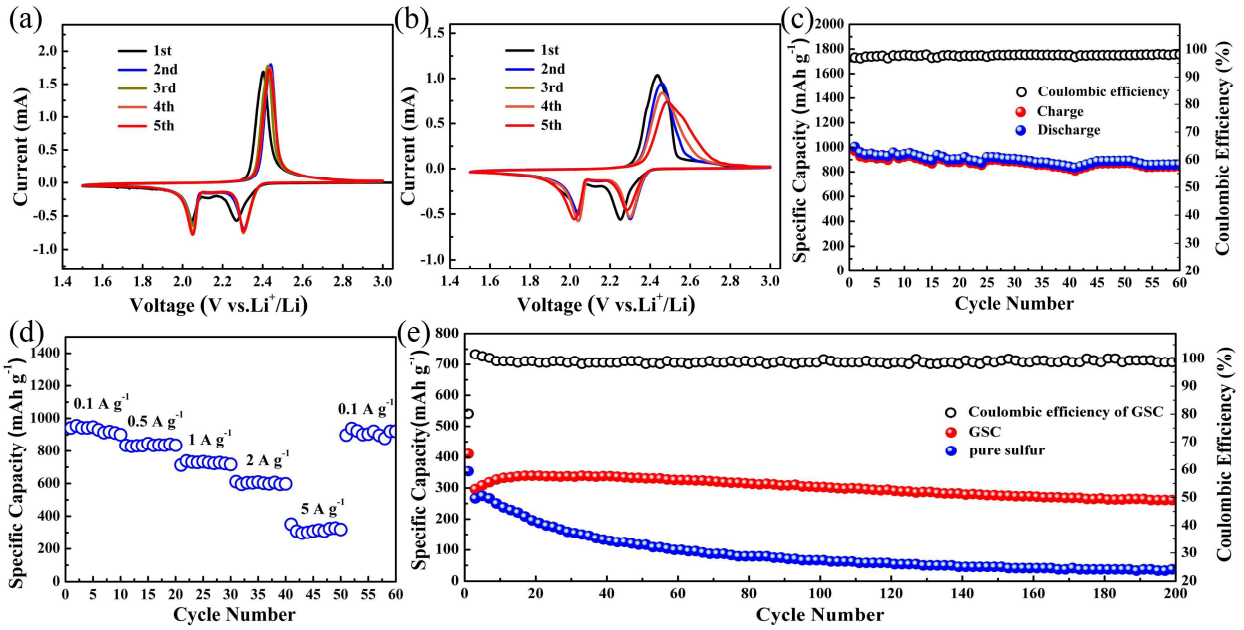

Figure 6. CV curves of GSC (a) and pure sulfur (b) measured over the potential window of 1.5-3.0 V at a scan rate of 0.1 mV s^{-1}. (c) Cycling performance of GSC. (d) Rate performance of GSC. (e) Long cycling performance of GSC and pure sulfur at 5 A g^{-1}.

into the *in situ* exfoliated graphene. More importantly, the sulfur electrodeposition at the electrode/electrolyte interfaces can ensure the sulfur particles intimate contact with the graphene sheets, effectively confining lithium polysulfides from dissolving. In order to further confirm the strong sulfur chemical interaction with the graphene hosts, the SEM images of GSC before and after cycling at 5 A g^{-1} are provided in Figure S4. After 200 cycles, the GSC still displays a homogeneous morphology. The GSC particles do not exhibit pulverization. The above facts indicate the strong graphene sulfur chemical interaction during repeated cycling, which consequently enhances the cyclic stability and rate capability. Therefore, the exfoliated flexible graphene sheets not only increase the conductivity but also accommodate the stress and volume expansion of the electrode during Li-S electrochemical reactions.

Figure 6d exhibits the rate capability of the GSC electrode at different current density from 0.1 to 5 A g^{-1}. A reversible capacity of around 850 mAh g^{-1} can be obtained at a current density of 0.5 A g^{-1}, owing to the good electrical conductivity of graphene and the uniformly dispersed S. The value is about 700 and 625 mAh g^{-1} for 1.0 and 2.0 A g^{-1}, respectively. A satisfactory capacity of 300 mAh g^{-1} can still be delivered when the current density increases to 5 A g^{-1}. Moreover, when the current density returns back to 0.1 A g^{-1}, the electrode can almost recover to its original capacity. This value is comparable to the best performance of graphene-sulfur cathode materials prepared by solution-chemical reaction-deposition method,[42] *in situ* solution deposition method[43] and other methods.[44–46] In addition, the long cycling performance of the GSC and pure sulfur electrode at a high rate of 5 A g^{-1} is provided in Figure 6e. The GSC exhibits a much better cycling performance than pure sulfur electrode.

Conclusions

In summary, a novel strategy *via* electrochemical exfoliation-deposition reactions at electrode/electrolyte interfaces has been developed to fabricate the GSC with uniform distribution and high content of sulfur. This facile route can provide the strong sulfur chemical interaction with the graphene hosts, enables us to obtain uniform graphene-wrapped sulfur particles. Therefore, the as-formed GSC electrode delivers an initial discharge capacity of 1080 mAh g^{-1} at 0.1 A g^{-1} and retains higher than 900 mAh g^{-1} over 60 cycles. As expected in the future, it will be of significant interest to explore sulfur-based composites by the electrodeposition of sulfur on various hosts such as porous carbon or conductive polymer nanocomposite cathodes for advanced Li/S cells.

Acknowledgement

This work was supported by National Natural Science Foundation of China (no. 51201151, 51172205 and 201403196), Natural Science Foundation of Zhejiang Province (LR13E020002 and LY13E020010), Visiting Scholar Foundation from State Key Lab of Silicon Materials, Zhejiang University (SKL2014-2), Scientific Research Foundation of Zhejiang Provincial Education Department (Y201432424) and Ford Motor Company.

Notes and references

1 X. Liang, C. Hart, Q. Pang, A. Garsuch, T. Weiss, L. F. Nazar, *Nat. Commun.*, 2015, **6**, 5682.

2 X. Y. Tao, J. G Wang, Z. G Ying, Q. X. Cai, G. Y. Zheng, Y. P. Gan, H. Huang, Y. Xia, C. Liang, W. K. Zhang, Y. Cui, *Nano Lett.,* 2014, **14**, 5288–5294.
3 Y. Yang, G. Y. Zheng, Y. Cui, *Chem. Soc. Rev*., 2013, **42**, 3018–3032.
4 N. Jayaprakash, J. Shen, S. S. Moganty, A. Corona, L. A. Archer, *Angew. Chem. Int. Ed*., 2011, **50**, 5904–5908.
5 X. L. Ji, K. T. Lee, L. F. Nazar, *Nat. Mater.*, 2009, **8**, 500–506.
6 Y. V. Mikhaylik, J. R. Akridge, *J. Electrochem. Soc*., 2004, **151**, A1969–A1976.
7 X. Y. Tao, X. R. Chen, Y. Xia, H. Huang, Y. P. Gan, R. Wu, F. Chen, W. K. Zhang, *J. Mater. Chem. A*, 2013, **1**, 3295–3301.
8 W. Zheng, Y. W. Liu, X. G. Hua, C. F. Zhang, *Electrochim Acta*, 2006, **51**, 1330–1335.
9 L. C. Yin, J. L. Wang, F. J. Lin, J. Yang, Y. N. Nuli, *Energy Environ. Sci*., 2012, **5**, 6966–6972.
10 L. F. Xiao, Y. L. Cao, J. Xiao, B. Schwenzer, M. H. Engelhard, L. V. Saraf, Z.M. Nie, G.J. Exarhos, J. Liu, *Adv. Mater*., 2012, **24**, 1176–1181.
11 N. Tachikawa, K. Yamauchi, E. Takashima, J. W. Park, K. Dokko, M. Watanabe, *Chem. Commun*., 2011, **47**, 8157–8159.
12 C. F. Zhang, H. B. Wu, C. Z. Yuan, Z. P. Guo, X. W. Lou, *Angew. Chem. Int. Ed*., 2012, **51**, 9592–9595.
13 R. Elazari, G. Salitra, A. Garsuch, A. Panchenko, D. Aurbach, *Adv. Mater*., 2011, **23**, 5641 –5644.
14 Y.S. Su, A. Manthiram, *Chem. Commun*., 2012, **48**, 8817–8819.
15 S. Dorfler, M. Hagen, H. Althues, J. Tubke, S. Kaskel, M. J. Hoffmann, *Chem. Commun*., 2012, **48**, 4097–4099.
16 S. Stankovich, D. A. Dikin, G. H. B. Dommett, K. M. Kohlhaas, E. J. Zimney, E. A. Stach, R. D. Piner, S. B. T. Nguyen, R. S. Ruoff, *Nature*. 2006, **442**, 282–286.
17 H. Wang, Y. Yang, Y. Liang, J. T. Robinson, Y. Li, A. Jackson, Y. Cui, H. Dai, *Nano Lett*., 2011, **11**, 2644–2647.
18 Y. Cao, X. Li, I. A. Aksay, J. Lemmon, Z. Nie, Z. Yang, J. Liu, *Phys. Chem. Chem. Phys*., 2011, **13**, 7660–7665.
19 S. Evers, L. F. Nazar, *Chem. Commun*., 2012, **48**, 1233–1235.
20 X. Y. Tao, J. T Zhang, Y. Xia, H. Huang, J. Du, H. Xiao, W. K. Zhang, Y. P. Gan, *J. Mater. Chem. A*. 2014, **2**, 2290–2296.
21 J. Guo, Y. Xu, C. Wang, *Nano Lett*., 2011, **11**, 4288–4294.
22 K. Li, B. Wang, D. Su, J. Park, H. Ahn, G. Wang, *J. Power Sources*. 2012, **202**, 389–393.
23 L. W. Ji, M. M. Rao, S, Aloni, L. Wang, E. J. Cairns, Y. G. Zhang, *Energy Environ. Sci*., 2011, **4**, 5053–5059.
24 M. Shamsipur, S. M. Pourmortazavi, M. Roushani, I. Kohsari, S. S. Hajimirsadeghi, *Microchim Acta*. 2011, **173**, 445–451.
25 E, Bura-Nakic, A. Róka, I. Ciglenecki, G. Inzelt, *J. Solid State Electrochem*., 2009, **13**, 1935–1944.
26 J. L. Zubimendi, R. C. Salvarezza, L. Vázquez, A. J. Arvia, *Langmuir*. 1996, **12**, 2–11.
27 B. Li, S. Li, J. Liu, B. Wang, S. Yang, *Nano Lett*. 2015, **15**, 3073–3079.
28 M. Yu, A. Wang, F. Tian, H. Song, Y. Wang, C. Li, J. D. Hong, G. Shi, *Nanoscale*, 2015, **7**, 5292–5898.
29 C. Y. Su, A. Y. Lu, Y. P. Xu, F. R. Chen, A. N. Khlobystov, L. J. Li, *ACS Nano*. 2011, **5**, 2332–2339.
30 M. Alanyalıoğlu, J. J. Segura, J. Oró-Solè, N. Casañ-Pastor, *Carbon*. 2012, **50**, 142–152.
31 J. Z. Wang, K. K. Manga, Q. L. Bao, K. P. Loh, *J. Am. Chem. Soc*., 2011, **133**, 8888–8891.
32 H. Huang, Y. Xia, X. Y. Tao, J. Du, J. W. Fang, Y. P. Gan, W. K. Zhang, *J. Mater. Chem.*, 2012, **22**, 10452–10456.
33 D. W. Wang, Q. C. Zeng, G. M. Zhou, L. C. Yin, F. Li, H. M. Chen, I. R. Gentl, G. Q. Max Lu, *J. Mater. Chem. A*. 2013, **1**, 9382–9394.
34 A. G. Schaufuss, H. W. Nesbitt, I. Kartio, K. Laajalehto, G. M. Bancroft and R. Szargan, J. Electron Spectrosc. Relat. Phenom., 1998, **96**, 69.
35 M. S. Park, J. S. Yu, K. J. Kim, G. Jeong, J. H. Kim, Y. N. Jo, U. Hwang, S. Kang, T. Woo and Y. J. Kim, Phys. Chem. Chem. Phys., 2012, **14**, 6796.
36 C. Wang, Z. Guo, W. Shen, A. Zhang, Q. Xu, H. Liu, Y. Wang, *J. Mater. Chem. A,* 2015, **3**, 6064–6072.
37 C. Zhang, Y. Lina, J. Liu, *J. Mater. Chem. A,* 2015, **3**, 10760–10766.
38 F. Gao, D. Zeng, Q. Huang, S. Tian, C. Xie, *Phys. Chem. Chem. Phys*. 2012, **14**, 10572.
39 L. Zhang, L. Ji, P.-A. Glans, Y. Zhang, J. Zhu, J. Guo, *Phys. Chem. Chem. Phys*. 2012, **14**, 13670.
40 J. Schuster, G. He, B. Mandlmeier, T. Yim, K. T. Lee, T. Bein, L. F. Nazar, *Angew. Chem. Int. Ed*., 2012, **51**, 3591 –3595.
41 S. Y. Zheng, Y. Wen, Y. J. Zhu, Z. Han, J. Wang, J. H. Yang, *Adv. Energy Mater*., 2014, 1400482.
42 H. Xu, Y. Deng, Z. Shi, Y. Qian, Y. Meng, G. Chen, *J. Mater. Chem. A*, 2013, **1**, 15142–15149.
43 S. Liu, K. Xie, Z. Chen, Y. Li, X. Hong, J. Xu, L. Zhou, J. Yuan, C. Zheng, *J. Mater. Chem. A*, 2015. **3**. 11395–11402.
44 G. Y. Zheng, Y. Yang, J. J. Cha, S. S. Hong, Y. Cui, *Nano Lett*., 2011, **11**, 4462–4467.
45 B. Zhang, X. Qin, G. R. Li, X. P. Gao, *Energy Environ. Sci*., 2010, **3**, 1531–1537.
46 R. Demir-Cakan, M. Morcrette, Gangulibabu, A. Guéguen, R. Dedryvère, J. M. Tarascon, *Energy Environ. Sci*., 2013, **6**, 176–182.
47

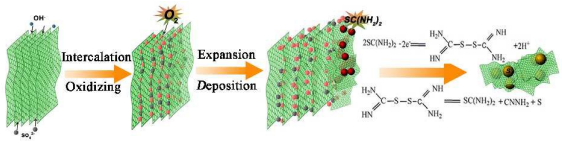

A novel synthesis of graphene-sulfur composites is designed by electrolytic exfoliation of graphite coupled with *in situ* electrodeposition of sulfur.